Atmos. Chem. Phys. Discuss., 15, 20629–20653, 2015
www.atmos-chem-phys-discuss.net/15/20629/2015/
doi:10.5194/acpd-15-20629-2015

Atmospheric Chemistry and Physics
Discussions
Open Access

Hydrolysis and gas-particle partitioning of organic nitrates formed from the oxidation of α-pinene in environmental chamber experiments

J. K. Bean and L. Hildebrandt Ruiz

McKetta Department of Chemical Engineering, The University of Texas at Austin, Austin, TX, USA

Received: 27 June 2015 – Accepted: 7 July 2015 – Published: 31 July 2015

Correspondence to: L. Hildebrandt Ruiz (lhr@che.utexas.edu)

Published by Copernicus Publications on behalf of the European Geosciences Union.

Abstract

Gas-particle partitioning and hydrolysis of organic nitrates (ON) influences their role as sinks and sources of NO_x and their effects on the formation of tropospheric ozone and organic aerosol (OA). Organic nitrates were formed from the photo-oxidation of α-pinene in environmental chamber experiments under varying conditions. A hydrolysis rate of 2 day^{-1} was found for particle-phase ONs at a relative humidity of 22 % or higher; no significant ON hydrolysis was observed at lower relative humidity. The ON gas-particle partitioning is dependent on total OA concentration and temperature, consistent with absorptive partitioning theory. In a volatility basis set the ON partitioning is consistent with mass fractions of [0 0.19 0.29 0.52] at saturations mass concentrations (C^*) of [1 10 100 1000] $\mu g\,m^{-3}$.

1 Introduction

Organic nitrates (ON) play an important role in atmospheric chemistry as they can act as sinks and sources of NO_x ($NO + NO_2$) and thereby affect the formation of tropospheric ozone and organic aerosol. The sink reaction – addition of NO to a peroxy radical (R-O-O•) to form an organic nitrate ($R\text{-}O\text{-}NO_2$) – breaks the •OH initiated oxidation cycle and reduces the formation of ozone (Seinfeld and Pandis, 2006). Most $R\text{-}O\text{-}NO_2$ molecules are semi-volatile and are therefore expected to partition between the gas and particle phases. They can be transported in either phase and can become a source of NO_x when they are photolyzed or oxidized, contributing to the regional nature of NO_x pollution. Attempts to implement organic nitrate decomposition reactions in a chemical transport model which did not account for gas-particle partitioning of organic nitrates resulted in over-prediction of NO_x and ozone concentrations (Yarwood et al., 2012), consistent with an over-estimate of the strength of organic nitrates as NO_x sources.

Recent studies have suggested that organic nitrates in the condensed phase may undergo hydrolysis, leading to the formation of HNO_3 (Day et al., 2010; Darer et al., 2011; Hu et al., 2011; Liu et al., 2012; Browne et al., 2013; Jacobs et al., 2014; Rindelaub et al., 2015). This is a more permanent sink for NO_x and would decrease the regeneration of NO_x from organic nitrates. While these studies have found evidence for hydrolysis of aerosol-phase organic nitrates (ON^{aer}) it is not clear at which rate ON hydrolysis occurs. Correctly modeling organic nitrates and ozone formation depends on knowledge of the ON partitioning coefficient and hydrolysis rate.

While ON hydrolysis in the bulk phase has been studied for decades (Baker and Easty, 1950, 1952; Boschan et al., 1955) organic nitrate hydrolysis in atmospheric particles has only recently started to receive attention. Day et al. (2010) observed a decrease in particulate organic nitrates measured in coastal southern California under acidic conditions at high relative humidity and hypothesized hydrolysis as the cause. Browne et al. (2013) used ON hydrolysis to justify observations over the Boreal Forest of higher levels of HNO_3 despite higher production rates of organic nitrates. The chamber experiments performed by Liu et al. (2012) using trimethylbenzene (an anthropogenic volatile organic compound) as a precursor were the first to measure the hydrolysis of condensed organic nitrates.

The partitioning of organic nitrates to the particle phase is important to determine their fate as only condensed organic nitrates are expected to hydrolyze appreciably to HNO_3. Absorptive partitioning theory (Pankow, 1994; Donahue et al., 2006; Rollins et al., 2013; Rindelaub et al., 2015) has been used to describe the gas-particle partitioning of organic nitrates. Rollins et al. (2013) used partitioning data from the 2010 CalNex Campaign to find a volatility basis set distribution for ON observed at ambient aerosol concentrations. Rindelaub et al. (2015) observed the partitioning of organic nitrates formed from the ·OH initiated oxidation of α-pinene at various levels of relative humidity. However, other work has suggested that the partitioning of organic nitrates to the particle phase is irreversible (Perraud et al., 2012). The goals of this work were to form organic nitrates in controlled environmental chamber experiments from the OH·

initiated oxidation of α-pinene under high NO_x conditions and various relative humidity levels and:

1. Confirm that the gas-particle partitioning of organic nitrates is reversible and can therefore be modeled by absorptive partitioning theory.
2. Parameterize the gas-particle partitioning of organic nitrates.
3. Quantify the hydrolysis rate of organic nitrates.

2 Methods

2.1 Environmental chamber experiments

All experiments were performed in the Atmospheric Physicochemical Processes Laboratory Experiments (APPLE) chamber located at the University of Texas at Austin (UT-Austin). The APPLE chamber is a $\sim 12\,m^3$ Teflon® bag suspended inside of a temperature-controlled room. The walls of the room are lined with UV lights which can be used to induce photolysis reactions. The intensity of the UV lights has been characterized by the photolysis rate of NO_2, which was measured to be $0.4\,min^{-1}$, similar to the expected ambient NO_2 photolysis rate (e.g. $0.46\,min^{-1}$ at a zenith angle of 40°, Carter et al., 2005). Before each experiment the bag was flushed for at least 12 h with clean air from an Aadco clean air generator (Model 737-14A) at a flow rate exceeding 100 liters per minute (LPM). Ammonium sulfate ($(NH_4)_2SO_4$) particles (Fisher Scientific, 99.5 %) were injected both to monitor wall loss rates (Hildebrandt et al., 2009) as well as to act as seed particles onto which organic vapors can condense. Gas phase NO was injected directly into the chamber from a cylinder (Airgas, 9.94 PPM ±2 %) and liquid-phase α-pinene (Sigma Aldrich, 98 %) was injected to a glass bulb and subsequently evaporated into the chamber with a steady stream of mildly heated air. H_2O_2, which photolyzes to 2•OH, was used as •OH radical source and was either injected by bubbling air through an aqueous H_2O_2 solution (Fisher Scientific, 30 % weight) or by injecting H_2O_2 solution into a glass bulb and subsequently evaporate it into the chamber with a steady stream of mildly heated air. Some experiments were performed under dry conditions (< 5 % relative humidity); in other experiments humidity was increased by passing air through clean water and then into the chamber. Experimental conditions and results are summarized in Table 1. Results are discussed in Sect. 3.

Reactions were allowed to proceed for at least 4 h with continuous UV light. In some cases the temperature effects on gas-particle partitioning were observed by increasing temperature to 40 °C in the chamber after the UV lights had been turned off (see Sect. 3.2).

2.1.1 Instrumentation

The composition of PM_1 (particulate matter smaller than 1 µm in diameter) was measured using an Aerosol Chemical Speciation Monitor (ACSM) from Aerodyne (Ng et al., 2011). In the ACSM, particles are flash-vaporized on a heater at 600 °C, and the resulting gas molecules are then ionized using electron-impact ionization. This harsh ionization method results in fragmentation of most molecules. The molecular fragments, which are measured by a quadrupole mass spectrometer, are attributed to four categories – organics, nitrate, sulfate, and ammonium – using a fragmentation table (Allan et al., 2004). The instrument alternates between normal sampling and sampling through a particle filter, enabling subtraction of a gas-phase background. During this study the ACSM was operated at a time resolution (filter/sample cycle length) of approximately 90 s. The size distribution of particles was measured using a Scanning Electrical Mobility System (SEMS) from Brechtel Manufacturing, Inc. The SEMS uses a Differential Mobility Analyzer (DMA) to size-select particles based on their electric mobility, which are then counted by a Condensation Particle Counter (CPC). The DMA continuously cycled between the voltages which select particles ranging from 5 to 1000 nm, resulting in a time resolution of the particle size distribution of approximately 60 s.

Gas phase reaction products were monitored using a High-Resolution Time-of-Flight Chemical Ionization Mass Spectrometer (HR-ToF-CIMS) from Aerodyne Research, Inc. The HR-ToF-CIMS uses softer chemical ionization which results in minimal fragmentation of parent molecules. Mass spectra are derived from measurements of the ions' time-of-flight as they are pulsed through a low pressure chamber in a "V" shape. Two chemical reagent ions were used – water clusters ($H_3O^+ \cdot (H_2O)_n$) and iodide-water clusters ($I^- \cdot (H_2O)_n$). Water cluster ionization is most sensitive towards detection of moderately oxidized hydrocarbons; the ability to ionize and thus sensitivity is based on the relative proton affinity between the water cluster and the parent molecule (Lindinger et al., 1998). This method was used to monitor α-pinene as well as early-generation oxidation products. Iodide-water cluster ionization is most sensitive towards detection of more highly oxidized hydrocarbons; this method was used to observe later-generation oxidation products as well as HNO_3 and H_2O_2. In the work presented here data from the HR-ToF-CIMS are only used qualitatively since, as it was later discovered, a partially clogged inlet interfered with instrument calibration and quantitative measurements.

Concentrations of NO and O_3 were measured using Teledyne chemiluminescence NO_x and O_3 monitors (200E and 400E, respectively); concentrations of NO_2 were measured via an NO_2 monitor from Environnement (Model AS32M), which uses a Cavity Attenuated Phase Shift (CAPS) method to directly measure NO_2 (Kebabian et al., 2008). The advantage of this direct NO_2 measurement is that it does not rely on NO_2 conversion to NO and therefore does not suffer from interference by other oxidized nitrogen compounds such as HONO and organic nitrates (Winer et al., 1974).

2.1.2 Data analysis

Data from the ACSM were analyzed in Igor Pro using the software package "ACSM Local," which includes a correction for relative ion transmission efficiency as well as changes in the flow rate throughout the experiment. The SEMS volume concentration was converted to mass using the densities 1.77 $g\,cm^{-3}$ for ammonium sulfate and

$1.4\,\mathrm{g\,cm^{-3}}$ for organics and organic nitrates (Ng et al., 2007). The time series of particle mass concentration (not corrected for wall losses) during Expt. 7 is shown in Fig. S1; other experiments exhibited similar time series.

All PM nitrate (measured by the ACSM as NO^+ and NO_2^+ fragments) was assumed to be organic because no inorganic nitrate was introduced in these controlled experiments. Nitric acid is formed in the particle phase through hydrolysis as well as in the gas phase, but it is assumed that nitric acid concentrations are negligible in the particle phase due to its high vapor pressure (Fry et al., 2009).

The ACSM does not detect all sampled particles, primarily due to particle bounce at the vaporizer, resulting in a collection efficiency (CE) smaller than 1. Collection efficiency and wall losses were accounted for simultaneously by multiplying the ACSM concentrations of organics and organic nitrates by the mass concentration ratio $C_{\mathrm{SEMS}}^{t=0}/C_{\mathrm{ACSM}}^{\mathrm{seed}}(t)$ as has been done in previous work (Hildebrandt et al., 2009). Here, $C_{\mathrm{SEMS}}^{t=0}$ is the mass concentration of ammonium sulfate seed just before the UV lights are turned on and organic aerosol formation commences and $C_{\mathrm{ACSM}}^{\mathrm{seed}}(t)$ is the time dependent mass concentration of $(NH_4)_2SO_4$ measured by the ACSM throughout the experiment. This correction assumes that particles on the chamber walls participate in gas-particle partitioning as though they are still in suspension and that the suspended ammonium sulfate concentration changes only due to wall losses. It accounts for partitioning of organic vapors into wall-deposited particles (Hildebrandt et al., 2009) but does not account for losses of organic vapors onto the clean Teflon® walls (e.g. Matsunaga and Ziemann, 2010).

The ACSM standard fragmentation table was adjusted based on filter measurements taken in each experiment as described in the Supplement. Data from the HR-ToF-CIMS were analyzed in Igor Pro (Wavemetrics) using Tofware, the software provided with the instrument. The data were first mass calibrated based on HR-ToF-CIMS reagent ions and other known ions. The baseline was subtracted and the average peak shape was found so it could be used for high resolution analysis, through which multiple ions can be identified at any given integer m/z. Ions up to m/z 300 were analyzed in high resolution mode. Only prominent ions were fit above m/z 200 because of the high number of possible ions at this high m/z. After ions were identified in the high resolution spectrum, the peaks were integrated to yield a time series of ions. Analyte ion concentrations were then normalized by the reagent ion concentrations – the sum of H_3O+, $H_3O+\cdot(H_2O)$ and $H_3O+\cdot(H_2O)_2$ for water cluster ionization and the sum of I^- and $I^-\cdot(H_2O)$ for iodide-cluster ionization. This correction accounts for changes in reagent ion concentrations and instrument sensitivity during and between experiments.

The partitioning coefficient of a species is defined as the ratio of the species concentration in the particle phase to the total species concentration (gas and particle phase). For a single compound the partitioning coefficient is the same whether it is on a mass or mole basis. However, for a mix of compounds, such as those formed in ·OH-initiated oxidation, the mass and mole-basis partitioning coefficients will be different, with the coefficient expected higher on a mass basis since higher molecular weight compounds typically have lower vapor pressure. The partitioning coefficient in this work was calculated on a mole basis, in part because fragmentation in the ACSM makes it impossible to tell the original size and identity of ON molecules. This mole-basis partitioning coefficient is also more useful for most modeling efforts which group chemical species without knowledge of their exact molecular identity. The particle-phase ON concentration was quantified using data from the ACSM: mass concentrations of NO^+ and NO_2^+ fragments measured by the ACSM were converted to mixing ratios (ppb) using the molecular weights of the fragments, and the sum of the PM NO^+ and NO_2^+ mixing ratios was used as the ON mixing ratio. This assumes that the ON have only one nitrate functional group. Conversion of the NO^+ and NO_2^+ mass concentrations to mixing ratios avoids the need to assume an ON molecular weight (needed to estimated ON mass concentrations from ACSM) and is therefore deemed to be a more accurate measure of ON from the ACSM. Quantification of all gas phase ON species would necessitate calibration and identification of all ON species which is not feasible. Instead, a chamber box model and nitrogen balance was employed to estimate total gas-phase ON as described below.

2.2 Chamber modeling and partitioning coefficient

In these experiments only five major forms of oxidized nitrogen are present – NO, NO_2, HNO_3, ON^{gas} and ON^{aer} (gas and aerosol-phase organic nitrates, respectively). Concentrations of NO and NO_2 were measured using gas-phase monitors, and ON^{aer} was measured using the ACSM. Concentrations of HNO_3 were approximated using the Statewide Air Pollution Research Center (SAPRC) box model (http://www.engr.ucr.edu/~carter/SAPRC/). The H_2O_2 concentration used in the model was adjusted until the modeled NO, NO_2, and O_3 concentrations closely matched those observed throughout each experiment as shown in Fig. S2 for Expt. 7. The modeled HNO_3 concentration was then used with the measured NO, NO_2, and ON^{aer} to find the ON^{gas} based on a nitrogen mass balance ($ON^{gas} = NO_x^{initial} - NO_2 - NO - ON^{aer} - HNO_3^{model}$). The partitioning coefficient ($ON^{aer}/ON^{aer} + ON^{gas}$) was then calculated as a time series for each experiment.

SAPRC simulations were conducted with the reaction mechanism Carbon Bond 6 revision 2 (CB6r2), which includes organic nitrate hydrolysis through a rate estimated from a combination of the work of Liu et al. (2012) and Rollins et al. (2013) (Hildebrandt Ruiz and Yarwood, 2013). Experiments were modeled with and without organic nitrate hydrolysis to see the effect this has on the predicted ON partitioning coefficient. The overall effect of this process in the model was small: in 80 % of the data points used (individual time points from each experiment) to find the volatility basis set (described below) the removal of the hydrolysis process in the model causes a decrease in the calculated partitioning coefficient of less than 5 %. The maximum decrease in partitioning coefficient (8.6 %) due to removal of the modeled hydrolysis process corresponded to a decrease in HNO_3 of 27 % at that particular time. This shows that the partitioning coefficient estimated in this work is not very sensitive to changes in the modeled HNO_3 concentrations. For the results and analysis presented here the HNO_3 concentrations were taken from CB6r2 with the inclusion of the ON hydrolysis process for experiments above 20 % RH and without the hydrolysis process for experiments below 20 % RH.

According to absorptive partitioning theory (Pankow, 1994; Donahue et al., 2006), the gas-particle partitioning of an organic species depends on its vapor pressure and the concentration of organic material already in the condensed phase. The fraction of a compound i in the particle phase (Y_i) is given by (Donahue et al., 2006):

$$Y_i = \left(1 + \frac{C_i^*}{C_{\mathrm{OA}}}\right)^{-1} \tag{1}$$

where C_{OA} is the organic aerosol concentration and C_i^* is the saturation mass concentration of species i (the saturation vapor pressure converted to concentration units). In the volatility basis set (VBS, Donahue et al., 2006), organic species are lumped by C_i^* spaced logarithmically. This leads to an overall partitioning coefficient

$$Y_{\mathrm{tot}} = \sum_{i=1}^{n} F_i \left(1 + \frac{C_i^*}{C_{\mathrm{OA}}}\right)^{-1} \tag{2}$$

(Rollins et al., 2013), where F_i is the fraction of organic species in the volatility bin described by C_i^*. In this work we used measurements of C_{OA} and Y_{tot} to fit the F_i using a Matlab optimization routine. These VBS parameters can be used in models to represent the gas-particle partitioning of organic nitrates and account for changes in partitioning with temperature and C_{OA}.

3 Results and discussion

A typical time series of compounds containing oxidized nitrogen is shown in Fig. 1 (Expt. 7). Initially the chamber contains only NO and a small amount of NO_2, in addition to α-pinene and inorganic seed aerosol. When the UV lights are activated at time = 0 the NO immediately begins to react with ·OH and other radicals to form NO_2

and additional NO_y compounds such as organic nitrates. Concentrations of ON^{aer} and ON^{gas} from all experiments are summarized in Table 1.

In high RH experiments (Expts. 4, 10 and 11) ON^{gas} concentrations calculated using this mass balance approach are very low and sometimes below zero. This could be caused by an overestimate of wall-loss corrected ON^{aer} concentrations at high relative humidity. The wall loss correction used here and in previous work (Hildebrandt et al., 2009) assumes that particles lost to the walls still participate in partitioning as though in suspension. This assumption may be poor if small amounts of water condense onto the walls of the chamber in high RH experiments. It is also possible that at high relative humidity HNO_3 partitions to the particle phase and is measured by the ACSM. In this case it would be double counted in the mass balance as both HNO_3 and as ON^{aer}, which would lower the estimates for ON^{gas}. Due to these issues with calculating the gas-phase ON concentrations in high RH experiments only low RH experiments are used for calculating the ON partitioning coefficient.

Figure 2 shows time series of selected molecular ions identified using the HR-ToF-CIMS using water cluster ("positive mode") and iodide-water cluster ("negative mode") ionization. The initial data collected in negative mode show that formation of organic nitrates begins immediately after oxidation has started. The less-oxygenated compounds observed in positive mode begin to decrease while the more highly oxygenated compounds observed in negative mode continue to increase, consistent with oxidation and conversion of less-oxidized compounds to more highly-oxidized compounds continuing throughout the experiment. Highly-oxidized compounds which still contain ten carbon atoms (as the precursor α-pinene) begin to decrease towards the end of the experiment while fragmented compound (containing less than ten carbon atoms) continue to increase, consistent with fragmentation of the carbon backbone during oxidation. Molecular weights of the gas-phase compounds identified here range from 221 to 279 $g\,mol^{-1}$ and align well with the range of molecular weights estimated by Fry et al. (2009) for particle-phase organic nitrates formed from NO_3 oxidation of α-pinene (229 ± 12 to

$434 \pm 25\,g\,mol^{-1}$). Gas-phase organic nitrates identified here are therefore expected to be semi-volatile and to partition significantly to the particle phase.

3.1 Gas-particle partitioning of organic nitrates

In order to test the reversibility of ON partitioning the temperature of the chamber was increased after OA had formed (and when the UV lights were off) in some experiments. Figure 3 shows gas and particle-phase measurements taken from a representative experiment (Expt. 2). After the UV lights are turned off there is a 60 min period in which the temperature stabilizes around 15 °C. This is followed by ~ 90 min of heating to a final temperature of 45 °C. After this the chamber is quickly cooled back to 15 °C. Figure 3b shows a time series of the Org/SO_4 and ON^{aer}/SO_4 ratios measured by the ACSM. Sulfate has a low vapor pressure and does not evaporate significantly at the temperatures investigated; therefore changes in the ON^{aer}/SO_4 and Org/SO_4 ratios with chamber temperature can be attributed to partitioning of organic nitrates and other organic species between the gas and particle phases. As Fig. 3b shows, Org/SO_4 and ON^{aer}/SO_4 decreased with increasing temperature and increased with decreasing temperature, suggesting evaporation of species at higher temperatures and their re-partitioning to the particle phase at lower temperatures.

Figure 3b shows the effects of temperature on various compounds measured in the gas phase. Several organic compounds – with and without ON functional groups – increase with increasing temperature. This suggests that these compounds are present in both the gas and particle phases and evaporate at higher temperature resulting in increased gas phase concentrations. As temperature is increased the percent change in the concentration of gas-phase $C_{10}H_{16}O_2$ is less than the change in $C_{10}H_{16}O_4$ and the percent change in the concentration of gas-phase $C_{10}H_{15}NO_4$ is less than the change in $C_{10}H_{15}NO_6$. This is consistent with the more highly oxidized compounds having a lower vapor pressure and evaporating less. As the temperature is decreased back to 15 °C the concentrations return to the pre-heating trends, suggesting that recondensation to the particle-phase has occurred. These observations, as well as the trends seen in particle-phase measurements are consistent with equilibrium partitioning and inconsistent with the irreversible partitioning of ON recently suggested by Perraud et al. (2012).

Table 1 summarizes results from all experiments. Each value in the table is an average over approximately 20 min of the time when PM organics and nitrates peak in concentration. We chose to compare the data at the maximum so that experiments with different H_2O_2 concentrations could be compared even though they reach their maximum concentrations at different rates. Higher initial loading of NO_x, α-pinene, and H_2O_2 results in higher ozone and PM concentrations. The average partitioning coefficient of ON for this time period in each experiment is also shown; a more detailed analysis of ON partitioning follows. As mentioned above gas-phase ON could not be estimated reliably for high RH experiments, and therefore Table 1 only shows partitioning coefficients for low RH experiments.

Data from the lower-concentration experiments (Expts. 1–3) were fit to a volatility basis set as these experiments were conducted under atmospherically relevant conditions. Experimental data were used after total PM organics (corrected for wall losses) had reached $2\,\mu g\,m^{-3}$ to avoid effects of noise and model uncertainty at the beginning of the experiments when concentrations of both gas- and particle-phase organic nitrates were low. Outlying points (for example, when PM organics temporarily jumped to above $2\,\mu g\,m^{-3}$ but subsequent data suggested that condensation had not begun) were removed as well. Figure 4a shows the data used to find the volatility basis set along with the fit. The C^* values used for this were 1, 10, 100, and $1000\,\mu g\,m^{-3}$; the corresponding mass fractions (F_i) = calculated to give the best fit for Eq. (2) (Sect. 2.2) are $F_i = 0$, 0.19, 0.29, and 0.52.

The data from higher concentration experiments (Expts. 5–9) is shown with the volatility basis set trace in Fig. 4b. The data selected are those from the time period from when the NO_x monitor reading of NO was first below 5 ppb to ten minutes after the peak of the corrected PM nitrate signal. The NO concentration of below 5 ppb was chosen to minimize any hysteresis effects of the NO monitor on the mass balance calculation of the partitioning coefficient (time delays in measurements were observed during calibrations of the Teledyne NO_x monitor). This was not needed for low concentration experiments because they were conducted with low H_2O_2 levels and slower resulting rates – minimizing the effects of hysteresis from the NO_x monitor. Data were only used up to the time of 10 min after the peak of PM nitrate to minimize effects of uncertainty in the wall loss correction, which increase over the course of an experiment. There is good agreement between the data points from these experiments and the volatility basis set which was found from only the lower concentration experiments.

These results indicate that under typical ambient conditions ($< 40\,\mu g\,m^{-3}$ of OA) 5–20 % partitioning of ON is expected. This is significantly lower than the organic nitrate partitioning coefficient calculated by Rollings et al. (2013) for organic nitrates measured in Bakersfield, CA during the CalNex campaign in 2010 as shown in Fig. 4. The difference could be attributed to differences in precursor molecules and levels of oxidation. Rollins et al. (2013) determined using the SPARC model (Hilal et al., 2003) that precursor molecules (a mix of C5–C15 VOCs) would need two stages of oxidative chemistry beyond the initial $\cdot OH + VOC$ to reach the point when they would partition at 19–28 % for a C_{OA} of $3\,\mu g\,m^{-3}$. Our chamber data using α-pinene as a precursor appears to be more volatile than that measured in Bakersfield during CalNex 2010.

3.2 Hydrolysis of organic nitrates

Concentrations of wall-loss corrected PM organics and nitrate were observed to decrease towards the end of most experiments. (The exception was Expt. 1, in which concentrations continued to increase.) These decreases of PM organics and PM nitrate are attributed to physical or chemical processes in the gas and aerosol phases, and an exponential decay was fit to the data to quantify the decay. A correlation is observed between the rate of this decay for PM nitrate and the relative humidity as shown in Fig. 5. The details for each experiment are found in Table 1. In the four experiments with an RH at 15 % or below there appears to be little or no disappearance of nitrate. However, for experiments with RH at 22 % and higher the nitrate loss rate is approximately 2 day^{-1}. The one exception to this is Expt. 10 (RH = 70 %), which exhibited a significantly higher decay rate, possibly due to effects of being near the deliquescence relative humidity for that particular aerosol.

Measuring the disappearance of nitrate with the ACSM assumes that HNO_3 formed through hydrolysis volatilizes, consistent with its high vapor pressure (Fry et al., 2009). If HNO_3 does not volatilize completely, this method would result in an underestimate of the ON hydrolysis rate.

These results are consistent with other studies of the organic nitrate hydrolysis rate. Liu et al. (2012) observed a trend similar to that shown in Fig. 5 in chamber experiments in which ON were formed through the oxidation of tri-methyl benzene using HONO as the ·OH and NO_x source. In those experiments, PM nitrate was found to have negligible loss rate below 20 % RH and a loss rate of 4 day^{-1} at 40 % RH and higher. Perring et al. (2009) estimated the lifetime of isoprene nitrates to be between 95 min and 16 h based on their branching ratio in isoprene ·OH oxidation.

As Table 1 shows, we conducted experiments at varying NO_x and α-pinene concentrations, relative humidity, and hydrogen peroxide (·OH radical source) levels, which resulted in different final concentrations of PM nitrate and total OA. Liu et al. (2012) suggested that a lower PM nitrate/OA ratio at higher RH could be due to ON hydrolysis. In these experiments, the correlation between the ratio of PM nitrate/total OA (measured when total OA was highest) and RH was very low ($R^2 = 0.02$). Thus, based on these experiments, differences in the observed final PM nitrate/OA could be due to experimental conditions other than relative humidity.

4 Conclusions

We give evidence that organic nitrates formed during the oxidation of α-pinene are hydrolyzed in the particle phase at a rate of 2 day^{-1} when RH is 22 % or higher. The gas-particle partitioning of ON determines their potential to hydrolyze. We find that partitioning of the ON is reversible and can be described by a volatility basis set where the mass fractions at saturation mass concentrations of 1, 10, 100, and 1000 $\mu g\,m^{-3}$ are 0, 0.190, 0.275, and 0.535, respectively.

The conversion of NO_x to organic nitrates affects local ozone production. Partitioning and hydrolysis of organic nitrates affect regional concentrations of organic particulate matter and ozone. The organic nitrate partitioning coefficient and hydrolysis rate from this work can be used to include these processes in chemical transport models and more accurately represent the effect of organic nitrates on concentrations of ozone and particulate matter.

The Supplement related to this article is available online at doi:10.5194/acpd-15-20629-2015-supplement.

Acknowledgements. This work was financed in part through a grant from the Texas Commission on Environmental Quality (TCEQ), administered by The University of Texas through the Air Quality Research Program (Project 12-012). The contents, findings opinions and conclusions are the work of the authors and do not necessarily represent findings, opinions or conclusions of the TCEQ. The work was also financed in part through a grant by the Texas Air Research Center (Project 312 UTA0132A).

References

Allan, J. D., Delia, A. E., Coe, H., Bower, K. N., Alfarra, M. R., Jimenez, J. L., Middlebrook, A. M., Drewnick, F., Onasch, T. B., Canagaratna, M. R., Jayne, J. T., and Worsnop, D. R.: A generalised method for the extraction of chemically resolved mass spectra from Aerodyne aerosol mass spectrometer data, J. Aerosol Sci., 35, 909–922, doi:10.1016/j.jaerosci.2004.02.007, 2004.

Baker, J. and Easty, D.: Hydrolysis of organic nitrates, Nature, 166, 156–156, doi:10.1038/166156a0, 1950.

Baker, J. and Easty, D.: Hydrolylic decomposition of esters of nitric acid. 1. General experimental techniques – alkaline hydrolysis and neutral solvolysis of methyl, ethyl, isopropyl, and tert-butyl nitrates in aqueous alcohol, J. Chem. Soc., 1193–1207, doi:10.1039/jr9520001193, 1952.

Boschan, R., Merrow, R. T., and Van Dolah, R. W.: The chemistry of nitrate esters, Chem. Rev., 55, 485–510, doi:10.1021/cr50003a001, 1955.

Browne, E. C., Min, K.-E., Wooldridge, P. J., Apel, E., Blake, D. R., Brune, W. H., Cantrell, C. A., Cubison, M. J., Diskin, G. S., Jimenez, J. L., Weinheimer, A. J., Wennberg, P. O., Wisthaler, A., and Cohen, R. C.: Observations of total $RONO_2$ over the boreal forest: NO_x sinks and HNO_3 sources, Atmos. Chem. Phys., 13, 4543–4562, doi:10.5194/acp-13-4543-2013, 2013.

Carter, W., Cockeriii, D., Fitz, D., Malkina, I., Bumiller, K., Sauer, C., Pisano, J., Bufalino, C., and Song, C.: A new environmental chamber for evaluation of gas-phase chemical mechanisms and secondary aerosol formation, Atmos. Environ., 39, 7768–7788, doi:10.1016/j.atmosenv.2005.08.040, 2005.

Darer, A. I., Cole-Filipiak, N. C., O'Connor, A. E., and Elrod, M. J.: Formation and stability of atmospherically relevant isoprene-derived organosulfates and organonitrates, Environ. Sci. Technol., 45, 1895–902, doi:10.1021/es103797z, 2011.

Day, D. A., Liu, S., Russell, L. M., and Ziemann, P. J.: Organonitrate group concentrations in submicron particles with high nitrate and organic fractions in coastal southern California, Atmos. Environ., 44, 1970–1979, doi:10.1016/j.atmosenv.2010.02.045, 2010.

Donahue, N. M., Robinson, A. L., Stanier, C. O., and Pandis, S. N.: Coupled partitioning, dilution, and chemical aging of semivolatile organics, Environ. Sci. Technol., 40, 2635–2643, doi:10.1021/es052297c, 2006.

Fry, J. L., Kiendler-Scharr, A., Rollins, A. W., Wooldridge, P. J., Brown, S. S., Fuchs, H., Dubé, W., Mensah, A., dal Maso, M., Tillmann, R., Dorn, H.-P., Brauers, T., and Cohen, R. C.: Organic nitrate and secondary organic aerosol yield from NO_3 oxidation of β-pinene evaluated using a gas-phase kinetics/aerosol partitioning model, Atmos. Chem. Phys., 9, 1431–1449, doi:10.5194/acp-9-1431-2009, 2009.

Hilal, S., Karickhoff, S., and Carreira, L.: Prediction of the vapor pressure boiling point, heat of vaporization and diffusion coefficient of organic compounds, QSAR Comb. Sci., 22, 565–574, doi:10.1002/qsar.200330812, 2003.

Hildebrandt, L., Donahue, N. M., and Pandis, S. N.: High formation of secondary organic aerosol from the photo-oxidation of toluene, Atmos. Chem. Phys., 9, 2973–2986, doi:10.5194/acp-9-2973-2009, 2009.

Hildebrandt Ruiz, L. and Yarwood, G.: Interactions between Organic Aerosol and NO$_y$, Austin, TX. Prepared for the Texas AQRP (Project 12-012), by the University of Texas at Austin, and ENVIRON International Corporation, Novato, CA, available at: http://aqrp.ceer.utexas.edu/projectinfoFY12_13/12-012/12-012FinalReport.pdf, 2013.

Hildebrandt Ruiz, L., Paciga, A. L., Cerully, K., Nenes, A., Donahue, N. M., and Pandis, S. N.: Aging of secondary organic aerosol from small aromatic VOCs: changes in chemical composition, mass yield, volatility and hygroscopicity, Atmos. Chem. Phys. Discuss., 14, 31441–31481, doi:10.5194/acpd-14-31441-2014, 2014.

Hu, K. S., Darer, A. I., and Elrod, M. J.: Thermodynamics and kinetics of the hydrolysis of atmospherically relevant organonitrates and organosulfates, Atmos. Chem. Phys., 11, 8307–8320, doi:10.5194/acp-11-8307-2011, 2011.

Jacobs, M. I., Burke, W. J., and Elrod, M. J.: Kinetics of the reactions of isoprene-derived hydroxynitrates: gas phase epoxide formation and solution phase hydrolysis, Atmos. Chem. Phys., 14, 8933–8946, doi:10.5194/acp-14-8933-2014, 2014.

Kebabian, P. L., Wood, E. C., Herndon, S. C., and Freedman, A.: A practical alternative to chemiluminescence-based detection of nitrogen dioxide: cavity attenuated phase shift spectroscopy, Environ. Sci. Technol., 42, 6040–6045, doi:10.1021/es703204j, 2008.

Lindinger, W., Hansel, A., Jordan, A., and Hansel, A.: Proton-transfer-reaction mass spectrometry (PTR – MS): on-line monitoring of volatile organic compounds at pptv levels, Chem. Soc. Rev., 27, 347–354, 1998.

Liu, S., Shilling, J. E., Song, C., Hiranuma, N., Zaveri, R. A., and Russell, L. M.: Hydrolysis of organonitrate functional groups in aerosol particles, Aerosol Sci. Tech., 46, 1359–1369, doi:10.1080/02786826.2012.716175, 2012.

Matsunaga, A. and Ziemann, P. J.: Gas-wall partitioning of organic compounds in a Teflon film chamber and potential effects on reaction product and aerosol yield measurements, Aerosol Sci. Tech., 44, 881–892, doi:10.1080/02786826.2010.501044, 2010.

Ng, N. L., Chhabra, P. S., Chan, A. W. H., Surratt, J. D., Kroll, J. H., Kwan, A. J., McCabe, D. C., Wennberg, P. O., Sorooshian, A., Murphy, S. M., Dalleska, N. F., Flagan, R. C., and Seinfeld, J. H.: Effect of NO$_x$ level on secondary organic aerosol (SOA) formation from the photooxidation of terpenes, Atmos. Chem. Phys., 7, 5159–5174, doi:10.5194/acp-7-5159-2007, 2007.

Ng, N. L., Herndon, S. C., Trimborn, A., Canagaratna, M. R., Croteau, P. L., Onasch, T. B., Sueper, D., Worsnop, D. R., Zhang, Q., Sun, Y. L., and Jayne, J. T.: An Aerosol Chemical Speciation Monitor (ACSM) for routine monitoring of the composition and mass concentrations of ambient aerosol, Aerosol Sci. Tech., 45, 780–794, doi:10.1080/02786826.2011.560211, 2011.

Pankow, J. F.: An absorption model of gas/particle partitioning of organic compounds in the atmosphere, Atmos. Environ., 28, 185–188, doi:10.1016/1352-2310(94)90093-0, 1994.

Perraud, V., Bruns, E. A., Ezell, M. J., Johnson, S. N., Yu, Y., Alexander, M. L., Zelenyuk, A., Imre, D., Chang, W. L., Dabdub, D., Pankow, J. F., and Finlayson-Pitts, B. J.: Nonequilibrium atmospheric secondary organic aerosol formation and growth., P. Natl. Acad. Sci. USA, 109, 2836–41, doi:10.1073/pnas.1119909109, 2012.

Perring, A. E., Bertram, T. H., Wooldridge, P. J., Fried, A., Heikes, B. G., Dibb, J., Crounse, J. D., Wennberg, P. O., Blake, N. J., Blake, D. R., Brune, W. H., Singh, H. B., and Cohen, R. C.: Airborne observations of total $RONO_2$: new constraints on the yield and lifetime of isoprene nitrates, Atmos. Chem. Phys., 9, 1451–1463, doi:10.5194/acp-9-1451-2009, 2009.

Rindelaub, J. D., McAvey, K. M., and Shepson, P. B.: The photochemical production of organic nitrates from α-pinene and loss via acid-dependent particle phase hydrolysis, Atmos. Environ., 100, 193–201, doi:10.1016/j.atmosenv.2014.11.010, 2015.

Rollins, A. W., Pusede, S., Wooldridge, P., Min, K.-E., Gentner, D. R., Goldstein, A. H., Liu, S., Day, D. A., Russell, L. M., Rubitschun, C. L., Surratt, J. D., and Cohen, R. C.: Gas/particle partitioning of total alkyl nitrates observed with TD-LIF in Bakersfield, J. Geophys. Res.-Atmos., 118, 6651–6662, doi:10.1002/jgrd.50522, 2013.

Seinfeld, J. H. and Pandis, S. N.: Atmospheric Chemistry and Physics, 2nd Edn., Wiley-Interscience, Hoboken, 2006.

Winer, A. M., Peters, J. W., Smith, J. P., and Pitts, J. N.: Response of commercial chemiluminescent NO-NO, analyzers to other nitrogen-containing compounds, Environ. Sci. Technol., 8, 1118–1121, doi:10.1021/es60098a004, 1973.

Table 1. Experimental conditions and summary of results.

Exp	initial α-pinene (ppb)	initial NO (ppb)	RH (%)	H_2O_2 conc in model (ppb)[a]	O_3 (ppb)	ON^{aer} ($\mu g\,m^{-3}$)[b]	PM Org ($\mu g\,m^{-3}$)[b]	ON^{gas} (ppb)	Part coeff	Hyd. (day^{-1})
1	38	30	22	100	90	7.1	97.3	9.2	0.37	NA[c]
2	38	44	39	60	48	6.6	69.8	10.0	0.33	2.16
3	38	44	0	40	48	6.7	65.2	11.8	0.32	0.00
4	128	114	68	600	206					2.43
5	128	126	22	900	326	74.5	919.6	30.4	0.65	1.82
6	128	119	50	500	244	40.6	492.3	37.2	0.45	1.94
7	128	119	15	200	210	53.8	530.5	19.0	0.68	0.19
8	77	83	0	1000	304	27.2	321.0	20.5	0.50	0.63
9	77	80	0	1500	330	22.9	292.0	20.3	0.46	0.18
10	51	50	70	600	175					6.86
11	38	39	70	200	74					2.54

[a] H_2O_2 concentration for which SAPRC model most closely approximated laboratory measurements of NO_x and O_3 as shown in Fig. S2.

[b] Corrected for wall-losses as described in Sect. 2.1.2.

[c] Not enough data once aerosol growth had stopped.

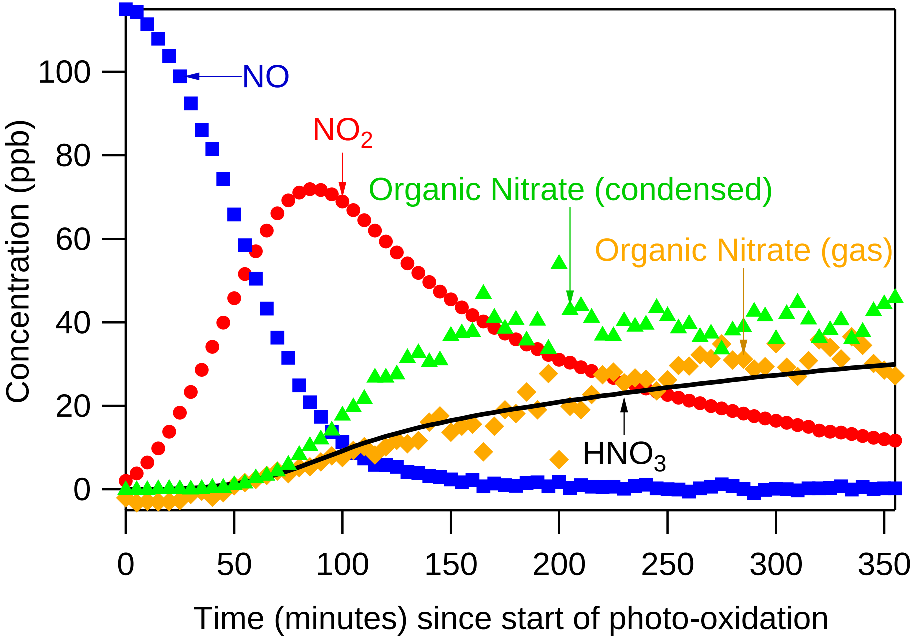

Figure 1. A time series of oxidized-nitrogen species in Expt. 7.

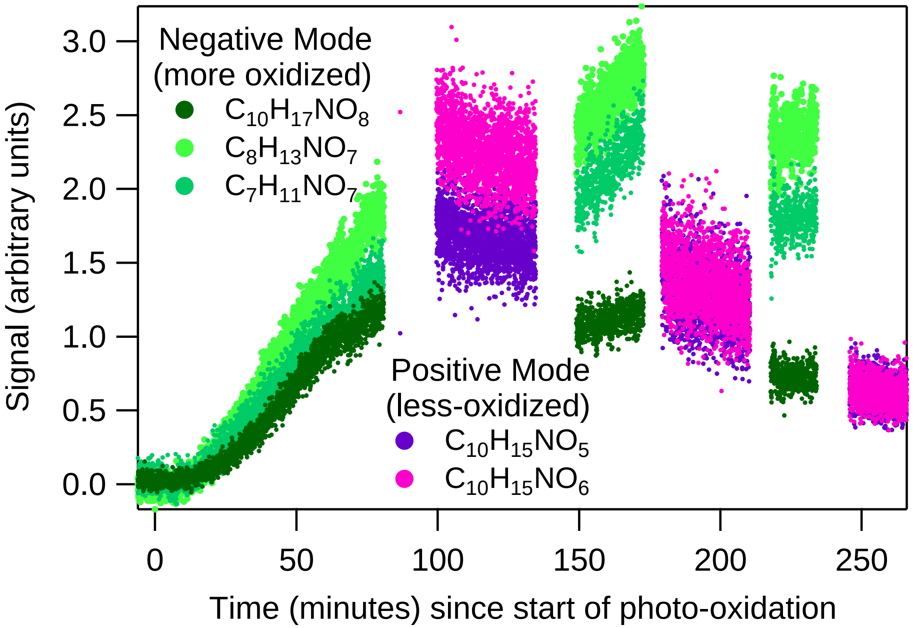

Figure 2. Time series of selected organic nitrates identified by HR-ToF-CIMS (Expt. 10).

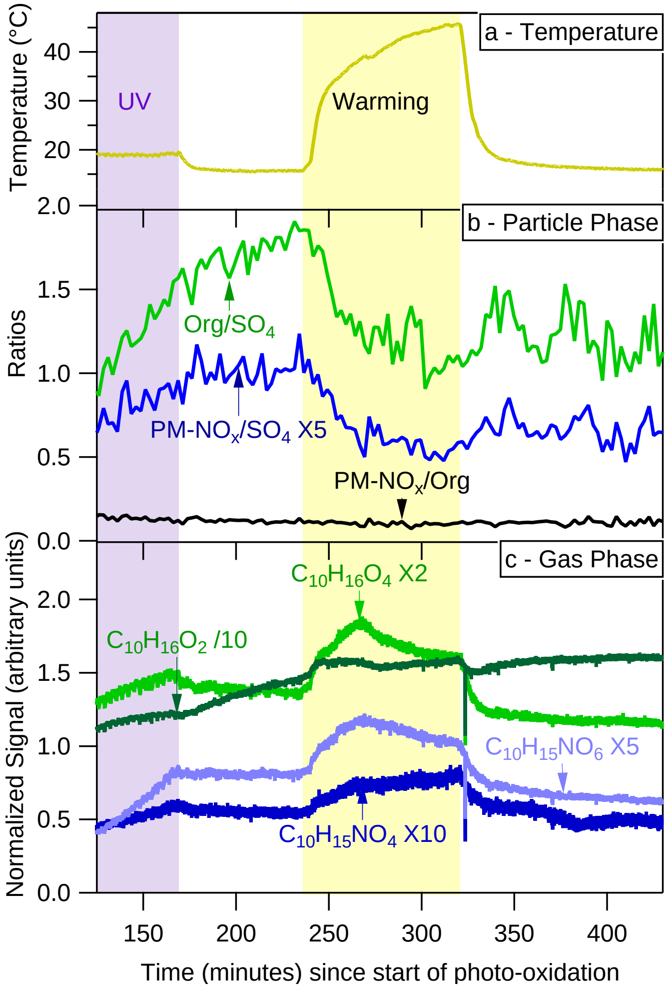

Figure 3. Temperature effects on gas-particle partitioning of organic nitrates (Expt. 2).

Title Page
Abstract | Introduction
Conclusions | References
Tables | Figures
I◀ | ▶I
◀ | ▶
Back | Close
Full Screen / Esc
Printer-friendly Version
Interactive Discussion

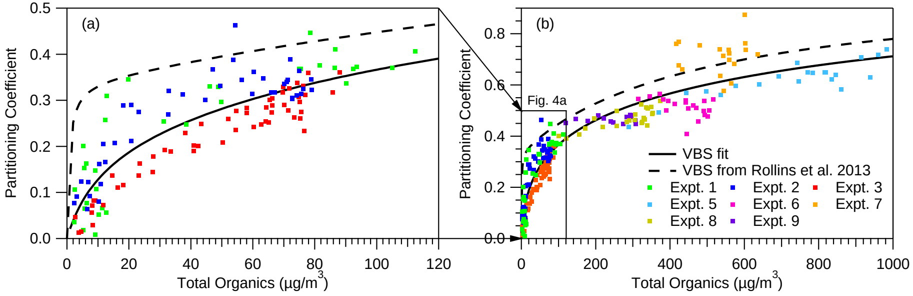

Figure 4. Volatility basis set fit from this work shown **(a)** with data from Expts. 1–3 and the VBS fit from Rollins et al. (2013) and **(b)** with data from Expts. 1–3 and 5–9 (RH 0–50 %).

Title Page
Abstract | Introduction
Conclusions | References
Tables | Figures
|◀ | ▶|
◀ | ▶
Back | Close
Full Screen / Esc
Printer-friendly Version
Interactive Discussion

ACPD
15, 20629–20653, 2015

Title Page
Abstract Introduction
Conclusions References
Tables Figures
◀▮ ▶▮
◀ ▶
Back Close
Full Screen / Esc
Printer-friendly Version
Interactive Discussion

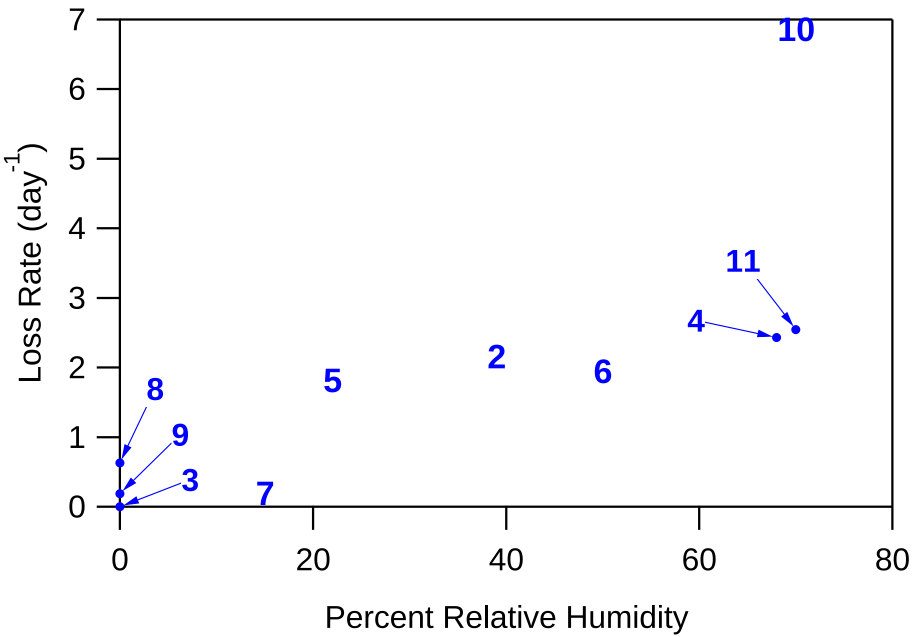

Figure 5. The organic nitrate loss rate as a function of relative humidity for Expts. 2–11.